Journal of the Indian Chemical Society 99 (2022) 100575

Contents lists available at ScienceDirect

Journal of the Indian Chemical Society

journal homepage: www.journals.elsevier.com/journal-of-the-indian-chemical-society

Green synthesis and characterization of Ag and Ag/Fe_3O_4 nanocomposites for antimicrobial effect and rhodamine- B dye degradation

K Saravanan [a], M. Ilayaraja [b,*], P. Muthukrishnan [c], S. Ananthakrishnan [a], P. Ravichandiran [a]

[a] Department of Chemistry, Roever Engineering College, Perambalur, 621212, Tamilnadu, India
[b] Department of Chemistry, Arumugam Pillai Seethai Ammal College, Tiruppattur, 630 211, Tamilnadu, India
[c] Department of Chemistry, Faculty of Engineering, Karpagam University (Karpagam Academy of Higher Education), Coimbatore, 641 021, Tamilnadu, India

ARTICLE INFO

Keywords:
Ag/Fe_3O_4 NCs
JC-Root
Green approach
Rhodamine B dye
Reusability

ABSTRACT

We used a simple two-stage tactic to design and synthesize a magnetically separable catalyst (MSC) Ag/Fe_3O_4 by combining independently synthesized Fe_3O_4 and Jatropha curcas root functionalized Ag nanoparticles (NPs) at room temperature. The phase composition of Ag/Fe_3O_4 NCs was revealed by morphological and structural assessment. The derived Ag/Fe_3O_4 nanocomposites demonstrated outstanding antimicrobial activity against Gram-negative Pseudomonas aeruginosa comparing to Gram-positive **Bacillus subtilis** which was determined by the agar well diffusion method. This is due to positively charged surface of metal oxide NPs that may bind to cell membrane. Interestingly, Ag–Fe_3O_4 NCs demonstrated good photocatalytic activity for organic dye degradation. According to a kinetic study, Ag/Fe_3O_4 MSC removed 99% of Rhodamine B at a rate constant of 1.89 min^{-1}. The photoelectron could perhaps ultimately collide only with dissolved solids in the substrate to form superoxides, which can damage the dye. Notably, the MSCs reusability was tested using magnetic detachment without sacrificing photocatalytic efficiency. This finding represents a significant breakthrough in the domain of wastewater treatment and biomedicine.

1. Introduction

Dyes are endocrine disruptors that are commonly used in garments, dosage form, pharmacy, and refining industries. Such dyes cause chronic, episodic, cancer causing, and oxidative stress on humans and livestock. In current history, colours are widely utilized colouring agents. Colour exposure has spread beyond the clothing industry which includes the fresh produce, printer ink, photocopying, beauty care, and drug companies [1–5]. The color scheme of the raw sewage causes an unsightly circumstance. Few of the colours are extremely complicated and hard to dwindle because of their complicated system and complex aroma. Furthermore, such colourants may be harmful to humans, carcinogenic, and neurotoxic as well have environmental impacts.

Azo Dyes are the synthetic dye form that ranges from red to violet in colour. It is frequently seen as a tracer colour in fluid to measure the rate and flow velocity and shipping. Rhodamine B (RB) ($C_{28}H_{31}ClN_2O_3$) is a well-known dye that is extensively utilized as a colourant in food stuffs and textile industries due to its high cohesion [6]. It is being used as a prototype chromophore. As the most important Xanthene dye and producing color hazardous emissions, both of which contribute to environmental concerns [7].

In latest generations, the emergence of new species of bacteria immune to existing antibiotics seems to have become a critical concern for living creatures. In these occasions, a recently possible approach is the use of magnetically recyclable processes. Magnetic nanoparticles renders significant contributions to current nanotechnology approaches, particularly ferromagnetic (Fe_3O_4) nanoparticles, which are regarded as excellent enhancing biomaterials matrices due to their favorable properties such as high magnetization, compact size, convenience of detachment, sensing, and targeted therapy [8,9] and also their low toxicity and biocompatibility.

Magnetostrictive drug designed to target with nanoparticles as carriers is a favorable chemotherapeutic agent that avoids the side impacts of various chemotherapeutic agents [10] Notwithstanding, magnetic nanoparticles and noble metal like biocatalytic composite materials has also recently received considerable attention due to its excellent attributes and promising effects in a variety of disciplines such as photocatalytic property [11], optoelectronic detector [12], biomedicine [13],

* Corresponding author.
E-mail addresses: saravananchemistry@gmail.com (K. Saravanan), ilayarajamsbm@gmail.com (M. Ilayaraja), mukepmk@gmail.com (P. Muthukrishnan), ananthajmc@gmail.com (S. Ananthakrishnan), ravichandiranpaul@gmail.com (P. Ravichandiran).

https://doi.org/10.1016/j.jics.2022.100575
Received 8 April 2022; Received in revised form 9 June 2022; Accepted 10 June 2022
Available online 18 June 2022

biocompatibility [14], and magnetic resonance imaging (MRI) contrast agents [15]. Furthermore, core shell nanoparticles have also sparked the fascination of engineers and scientists but it requires integrating the favorable characteristics of both core and shelling components [16]. Numerous chemically synthesized pathways have been utilized to enhance Ag/Fe_3O_4nanocomposites, such as the solution casting method [17], the solvo-thermal procedure [18], thermal decomposition [19], and the two-step chemical treatment [20]. The use of ecologically responsible and sustainable material for the production of metal nanoparticles was essential for biomedical applications.

The focus of this research was to assess the phytoremediation of Ag/Fe_3O_4NCs composed of Jatroba Curcus root aqueous extract and characterized as-synthesized nanocomposites. Subsequently, the photocatalytic profile of rhodamine dye removal and antibacterial action of synthesized Ag/Fe_3O_4NCs against clinical isolates of Bacillus subtilis (B. subtilis), Staphylococcus aureus (S. aureus), and Escherichia coli (E. coli), and Pseudomonas aeruginosa (P. aeruginosa) were appraised.

2. Components and processes

All of the designed mixtures was of analytical reagent grade and was utilized without any extra cleaning. Ferric chloride hexahydrate ($FeCl_36H_2O$), silver nitrate ($AgNO_3$), and sodium acidic destructive surmising were bought from Sigma Aldrich. The media utilized for bacterial social orders was from Hi-media, Mumbai, India. The Jatropha curcas root was collected from a nearby market on Karur Town, Tamilnadu, India. As of late set up, refined water was utilized for planning fluid strategies. AR grade ethanol (99.9%) was utilized for washing purpose.

2.1. Preparation of bio-chelating agent

The collected roots were thoroughly rinsed with a dual refined water to remove root debris, and then the roots were dehydrated under cover at room temperature for about 1 week in a dust-free environment. The dehydrated stems of Jatropha curcas root have been chopped into small pieces. A mixture of 5 g Jatropha curcas root powder and 100 mL of a dual refined water has been integrated and dialyzed for 1 h at 253 K until the diffusive concentrate grouping shifted from watery to light yellow. Eventually, the resulting mixture was cooled to room temperature and isolated using Whatman No. 1 channel paper, with the final precipitate being stored at room temperature for future use [21].

2.2. Fabrications of reusable magnetite nanoparticles

To make Ag/Fe_3O_4 NCs, 100 mg of Fe_3O_4 NPs and 50 mL of locally sourced Jatropha curcas root functionalized with Ag NPs solution were blended at ambient temperature with vigorous agitation until the homogeneous composition turned yellowish black in colour. The resulting suspension was centrifuged at 8000 rpm, and the solid residue was washed thoroughly with refined water multiple times in the applied magnetic field by employing a magnet. The scrubbed crude product was empowered to stand at room temperature overnight. The precipitate was then used to investigate the catalytic performance in the dye reduction process [22].

2.3. Hot filtration test

A hot filtration test was utilized after a 10–20% change of aryl iodide had been accomplished to guarantee that any filtered solvent Ag/Fe_3O_4 NCs in the filtrate would be adequate to proceed with a homogeneous response in the wake of eliminating the strong impetus.

2.4. Photocatalytic evaluation

To assess their photo catalytic efficiency under light irradiation, the

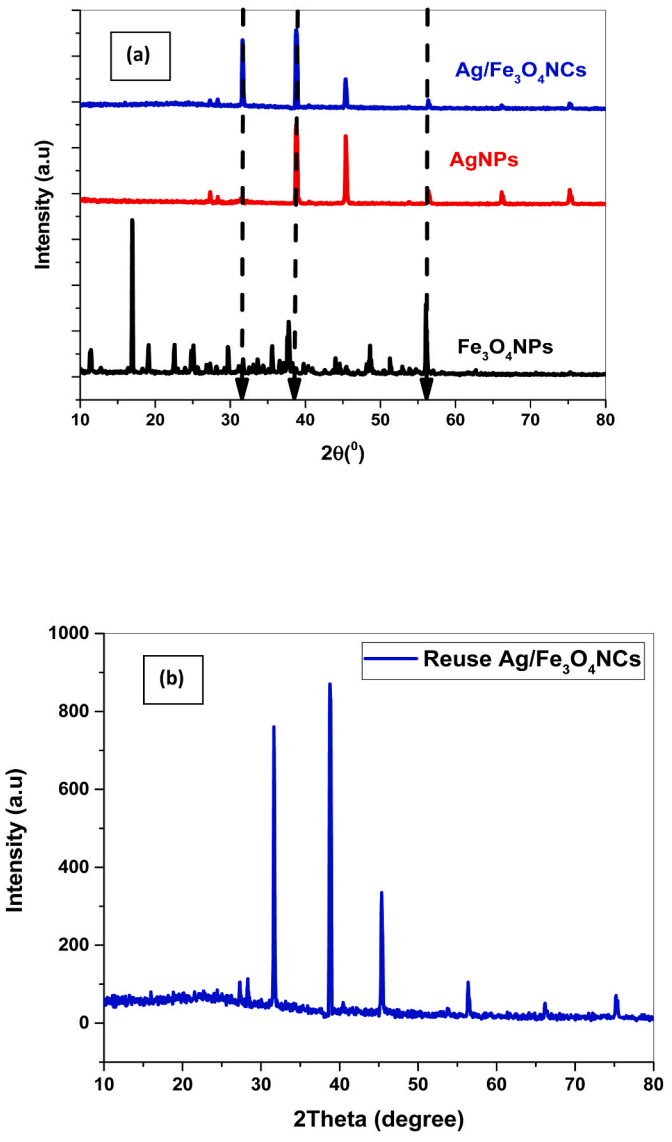

Fig. 1. (a) XRD pattern of synthesized (a) insitu Fe_3O_4 (b) AgNPs (c) Ag/Fe_3O_4 NCs (b) XRD patterns of Reused Ag/Fe_3O_4 NCs.

photo catalytic behavior of Ag/Fe_3O_4 nanocomposites has been examined employing Rhodamine B as the modal contaminant. To become more specific, 10 mg of the co-catalyst were mixed into 50 ml of Rhodamine B (10 ppm) aqueous medium. For about 15 min in a darkened room, the reaction solution was diluted and agitated to achieve adsorption – desorption approximation.

After exposing the reaction medium under visible light, the mixture was scraped out for every 30 min and the amounts of Rhodamine B dye were examined using UV–Vis Spectrophotometry. The efficiency of colour removal was measured in accordance with changes in intensity of the dye's assimilation ideal with reference to the amount released due to the illumination process. The degradation efficiency was predicted using the contaminant dye model [23].

$$(\%)\ Removal = ODControl - ODSample \,/\, ODControl \times 100 \quad (1)$$

2.5. Bactericidal activity

The anti-bacterial effect of the Ag/Fe_3O_4 NCs was evaluated against four microbial isolates, two Gram positive, Bacillus subtilis (B. subtilis), Staphylococcus aureus (S. aureus), and two Gram negative, Escherichia coli (E. coli), and Pseudomonas aeruginosa (P. aeruginosa). By

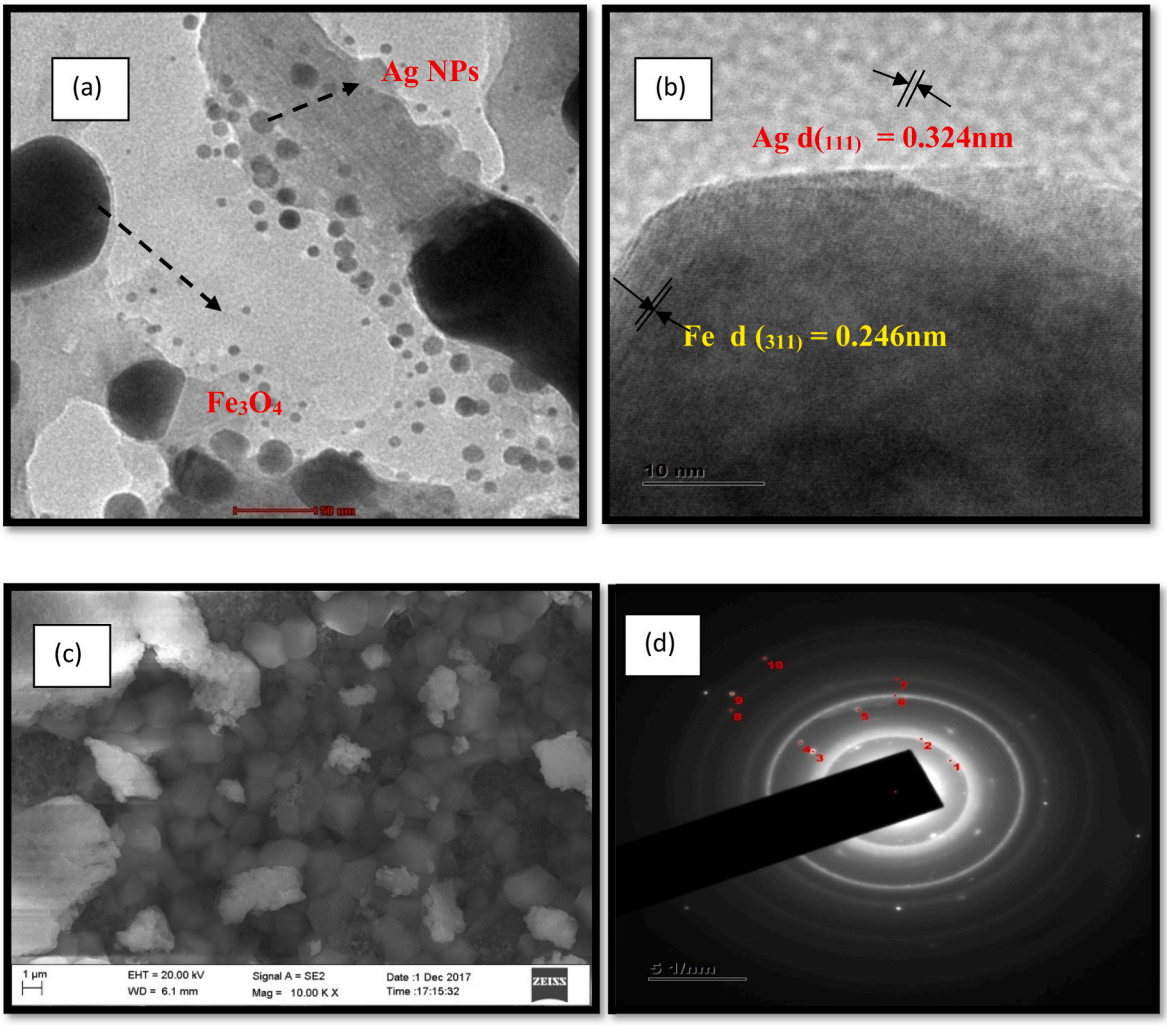

Fig. 2. (a) TEM profile (b) HRTEM microstructure (c) SEM profile (d) SEAD template.

distributing pathogenic bacteria isolates on the media, nutrient broth has been injected with the identified pathogens. Boreholes (9 mm diameter) have been thumped in the culture plate and loaded with 50, 75 and 100 µl of the synthesized Ag/Fe_3O_4 NCs. Streptomycin was evident in the control sample at a dose of 10 mg disc. Streptomycin has been used as a standard and incubated at 37 °C for 24 h. The zones of inhibition and demonstrated as mean Growth Inhibition in millimeter radius upon the incubation time [24].

3. Results and discussion

3.1. Crystal phase identification

The XRD behavior of Fe_3O_4 NPs was featured and additional details as shown in Fig. 1(a). The diffraction peak of Fe_3O_4 nanoparticles correlate to the Bragg's planes (220), (311), (400), (511) and (440), that also were in agreement with the inverse cubic spinel structure of Fe_3O_4 (magnetite, JCPDS File no. 15–1346). The presence of authorized Bragg's characteristic peaks in Fig. 1(a) insitu depicting the crystalline structure planes of (111), (200), (220), and (311) revealed the emergence of face-centered cubic Ag NPs (JCPDS no. 04–0643). The crystallinity estimated using Scherrer's model was 13 nm for Fe_3O_4 NPs and 12 nm for Ag NPs. The Powder x - ray crystalline structure of Ag/Fe_3O_4 NCs in Fig. 1(a) was extremely similar to that of genuine Fe_3O_4, with really no discernible crystallography peaks of Ag NPs. It could be attributable to the very modest amount of metallic Ag present in Fe_3O_4

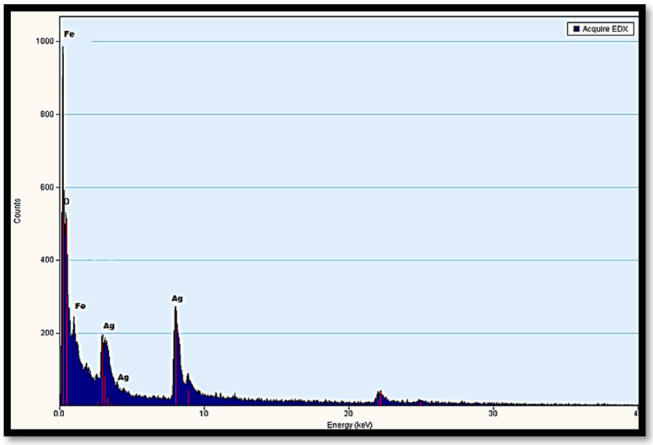

Fig. 3. EDX spectrum of Ag/Fe_3O_4 Nanocomposites.

crystallites [25–27]. The reuse of Ag/Fe_3O_4 NCs did not change in crystallite phase and purity of crystallite structure was shown in Fig- 1 (b).

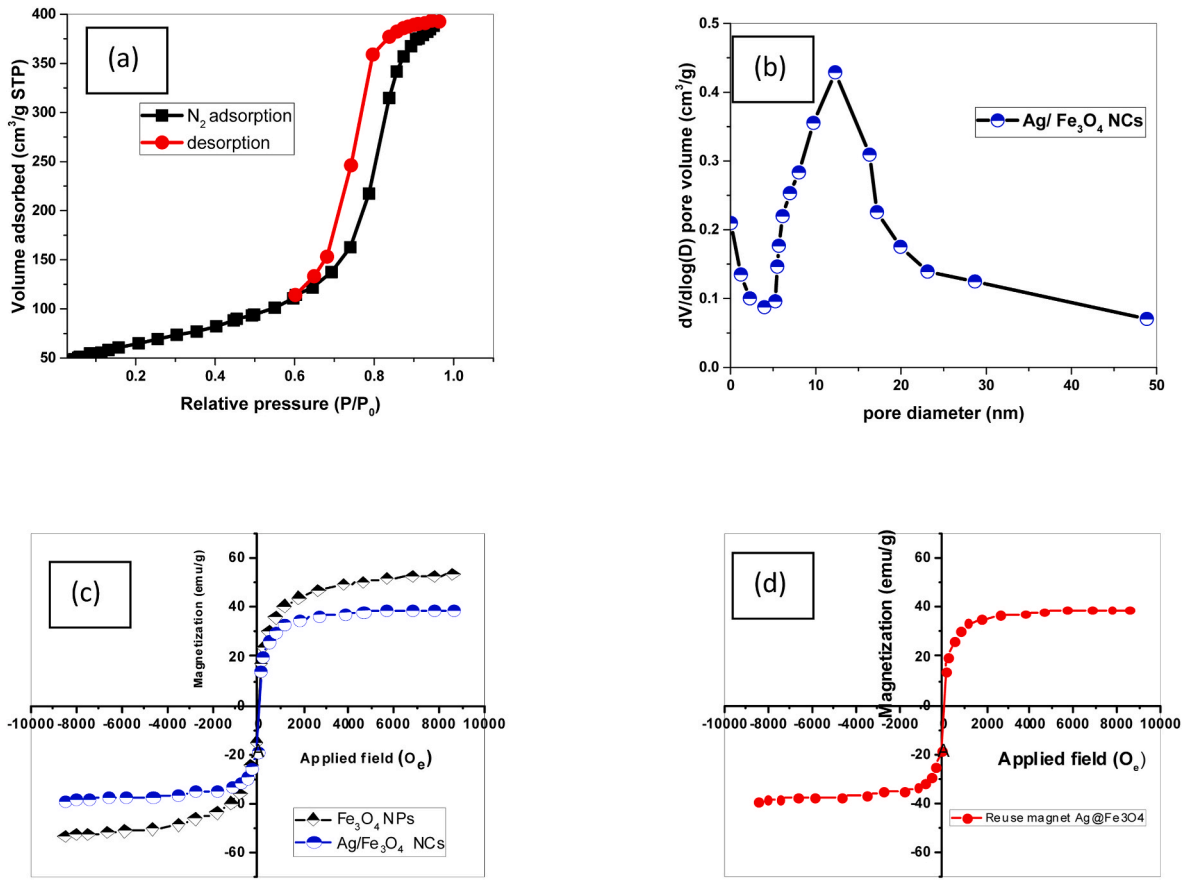

Fig. 4. (a) surface area analyze by BET isotherm (b) Pore area vs Pore volume (c) magnetic profile (d) reuse magnetic moment profile.

3.2. Assess of histological and elemental groups

TEM was used to examine the morphological characteristics of the Ag/Fe_3O_4 NCs core shell. Fig. 2(a) depicts almost the spherical structure with a size of less than 30 nm, while Fig. 2(b) represents the typical high-resolution TEM (HRTEM) appearance of the Ag/Fe_3O_4 NCs that comprised of two individual parts. The dark skinned core was crystalline Ag, and the grey shell was Fe_3O_4. Furthermore, the SAED template clearly shows nanoparticles' polycrystalline essence. Meanwhile, the polycrystalline constructive interference rings of the (1 1 1), (2 2 0), and (3 1 1) metrics of Fe_3O_4 inverse spinal structure and (1 1 1), (2 0 0) index of Ag face-centered cubic structure were visible in the correlating SEAD in Fig. 2(d). HRTEM interlayer spacing of Fe (0.246 nm) in Fig. 2(b) and Ag (0.324 nm) in Fig. 2(b) agreed with X-ray characteristic peaks of Ag and Fe_3O_4 NPs in the (111) and (220) planes, respectively.

As shown in Fig. 3, an energy dispersive X-ray (EDX) spectrum was obtained to determine the constituents of the probably resulted core shell nanoparticles. The essential components discovered were Fe, O, and Ag, indicating that the acquired nanocomposite was made up of the base material. These results demonstrated that Ag/Fe_3O_4 NCs can be successfully produced using a simple ecofriendly tactic.

3.3. BET isotherm and magnetic properties

Fig. 4 (a & b) depicts the N_2 adsorption behavior and average pore diameter of a fresh Ag/Fe_3O_4 catalyst. Fig. 4(a–b) illustrates that the genuine Ag/Fe_3O_4catalyst that displayed a type IV isotherm, which seems to be the conventional property of microporous materials [28]. The Brunauer–Emmett–Teller (BET) algorithm computed active interfacial region (SBET), as well as the volume dispersion in order to estimate the Barrett–Joyner–Halenda (BJH) approach formula and the adsorption equilibrium group. Figure −4 (a&b) illustrates that in all isotherm models, as the amount adsorption increased with the increase in about comparable pressure and predictions based on the volume filling of pore structure in the Fe_3O_4 substrate. Ag/Fe_3O_4 could have a BET particular accessible surface area radius of 12.14 m^2/g and pore diameter (Å) 0.049 cm^3/g, respectively [29].

3.4. Magnetic behavior

The magnetic characteristics of Fe_3O_4 NPs and Ag/Fe_3O_4 NCs at ambient temperature have been investigated utilizing VSM metrics. The saturation magnetization (Ms), residual magnetization (Mr), and coercive field (Hc) values for Ag/Fe_3O_4 NCs were 63.74 emu/g, 40.71 emu/g, and 389.39 G, respectively, implying that the nanocomposites exhibited ferromagnetic behavior. Nonzero residual magnetic moment (Mr) and coercive field (Hc) with non - linear curve confirmed ferromagnetic identity [30]. The permanent magnet reusability of Ag/Fe_3O_4 NCs in fluid was investigated by arranging an external magnet near the measuring cylinder. The materials were fascinated towards the magnet within seconds. Illustrations of Ag/Fe_3O_4 NCs diffusion prior to actually (a) and after (b) magnetic detachment are shown in Fig. 4 (c) & (d). As a byproduct, these magnetism nanoparticles could be used as repurpose materials in biomedical field in a fast and straightforward manner.

3.5. Optical properties analysis

Figure- 5 (a) depicts the UV–visible absorption spectra of Ag nanocolloids solution and Ag/Fe_3O_4 NCs. The detailed examination of the spectra of Ag colloidal particles revealed a broadband connection at 426 nm and a single SPR band of Ag/Fe_3O_4 NCs at 545 nm. The role and structure of exterior Photonic permeation of noble metal colloidal

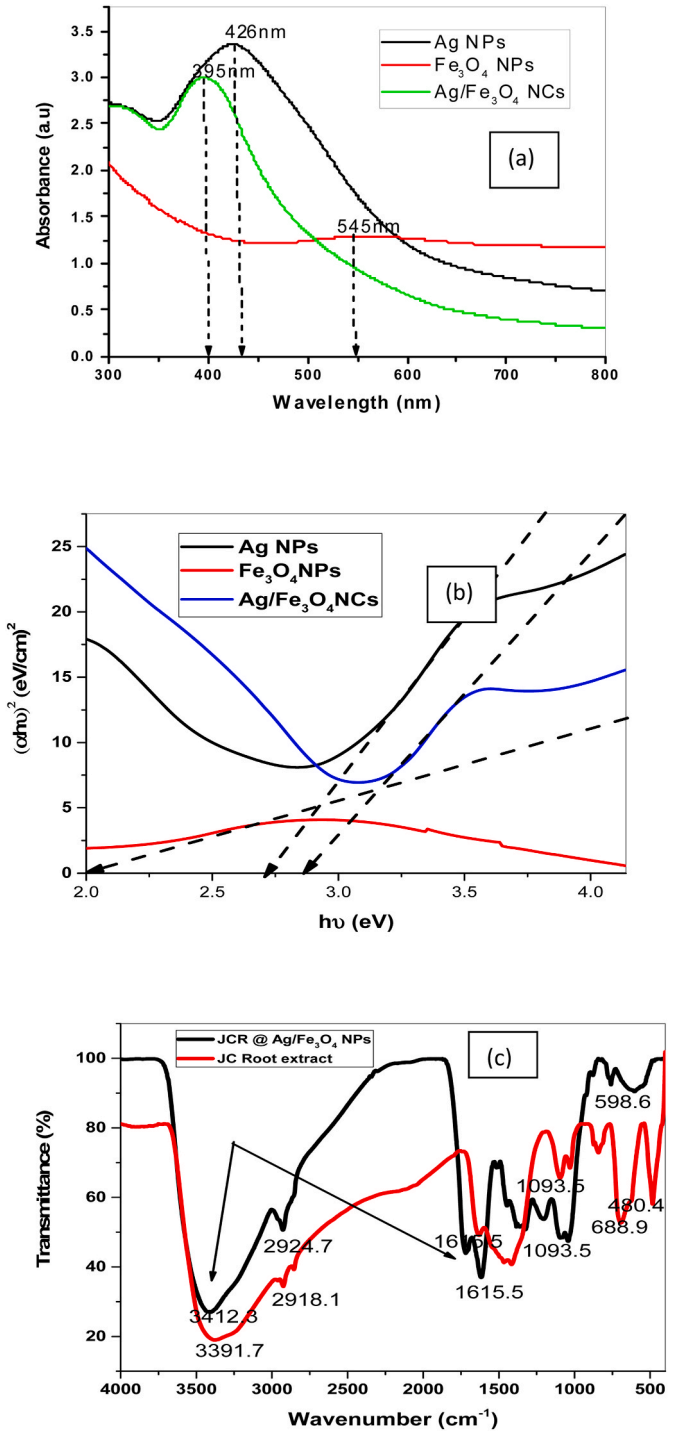

Fig. 5. (a) UV–visible absorption spectra and (b) Direct and indirect transition band gaps of Ag, Fe_3O_4 NPs and Ag/Fe_3O_4 NCs (c) Functional group analysis of Ag/Fe_3O_4 & JC Root Extract.

particles were hindered by size of particles and the ionic conduction in which they were suspended. Furthermore, impregnation of silver nanoparticles with dielectric properties caused a transformation in the SPR (surface plasmon resonance) peaks [31].

In comparison to genuine silver nanocolloids, Ag/Fe_3O_4 NCs exhibited a red shift. It was because of the dissipation factor assets of the Fe_3O_4enclosure, which would be accompanied by a silver core. As per Mie's concept [32], the above findings suggested that the biogenic synthesized Ag/Fe_3O_4 NCs were the integration of a light sprinkling Fe_3O_4 shell on the core of silver, which was consistent with the HRTEM and SAED effects.

3.6. Band gap

The band gap of Ag/Fe_3O_4 NCs was evaluated using Tauc relation

$$(\alpha \cdot h\nu)^{1/\gamma} = B(h\nu - Eg) \quad (2)$$

Where h is the Planck constant, ν is the photon's frequency, Eg is the band gap energy, and B is a constant. The γ factor depends on the nature of the electron transition and is equal to 1/2 or 2 for the direct and indirect transition band gaps is shown in Fig. 5 (b). The Eg of Ag/Fe_3O_4 NCs is 2.8 eV, which agreed with previous reports. The energy band gap value was responsible for the photocatalytic performance of textile dye damage.

3.7. Functional group analysis

FT-IR examination was completed to affirm the presence of phenolic intensifies in the concentrate, conceivable collaboration among biomolecules and Ag+ @ Fe^{3+}/Fe^{2+} particles for the union of Ag/Fe_3O_4 nanoparticles. The IR spectra of the unadulterated concentrate, Ag/Fe_3O_4 are displayed in Fig. 5 (c). The wide band focused at 3412.3 cm^{-1} of the unadulterated leaf separate is the quality of O–H extending mode for the Gracious gathering and the medium band saw at 1615.5 cm^{-1} relate to the ring extending method of C═C. The generally solid absorption at 1093 cm^{-1} could be assigned out to the C–O extending vibration of Gracious gathering, which uncovers the presence of phenolic intensifies in the concentrate. On account of Ag/Fe_3O_4 nanoparticles, a wide band decreased in the retention force with an unmistakable shift of ingestion tops was seen from 3412.3 to 3391.7 cm^{-1}, 1616 to 1615 cm^{-1} and 1093.7 to 1093.5 cm^{-1}, proposing that free Gracious gatherings of the mixtures in the concentrate have connected with Ag^+ @ Fe^{3+}/Fe^{2+} particles.

3.8. Photo catalytic activity upon rhodamine B dyes

The photocatalytic degradation of Ag/Fe_3O_4 nanocomposites was evaluated by observing the Rhodamine B (Rh–B) dye decomposes in the presence of visible light. The UV–Vis absorption spectra of the exposed samples were measured at successive periods as shown in Fig. 6(a–d). Rh–B dye was rapidly degraded in 110 min, which coincided to the photo - catalysts of Ag/Fe_3O_4 nanocomposites. Subsequently, the control experiment (blank) revealed that the breakdown was not realized due to lack of photo catalysts. Table-1 shows that comparison of various nanomaterials on rhodamine B dye.

3.8.1. Kinetic model

Fig. 6 b. depicts the kinetic pattern of Rhodamine B dye discharge as a function of light exposure with a fitted strong co-relation, implying pseudo-first kinetic parameters.

$$\ln (C_0 / C) = K_{app}t \quad (3)$$

Where K app t (min-1) is the apparent frequency constant and k is the pseudo rate constant, which has been expressed to be 1.89 min^{-1}. C_0 represents the dye's initial uptake, and C represents the uptake at duration. Henceforth, the regression analysis (R^2) of 0.99 confirmed that photo depletion of Rh–B dye follows the Langmuir–Hinshelwood kinetic template.

3.8.2. Light Perceived pathway on Dye Molecules

The holes were entangled by the H_2O to construct intense hydroxyl radicals (OH) and superoxide's ($O_2^{\cdot}$, $HO_2^{\cdot}$). Strong reactive oxygen species (ROS species such as OH and singlet oxygen (O_2, HO_2) may break down the organic dye. Ag NPs served as a photons sink, promoting interlayer transfer of electrons and reducing photo induced hole -

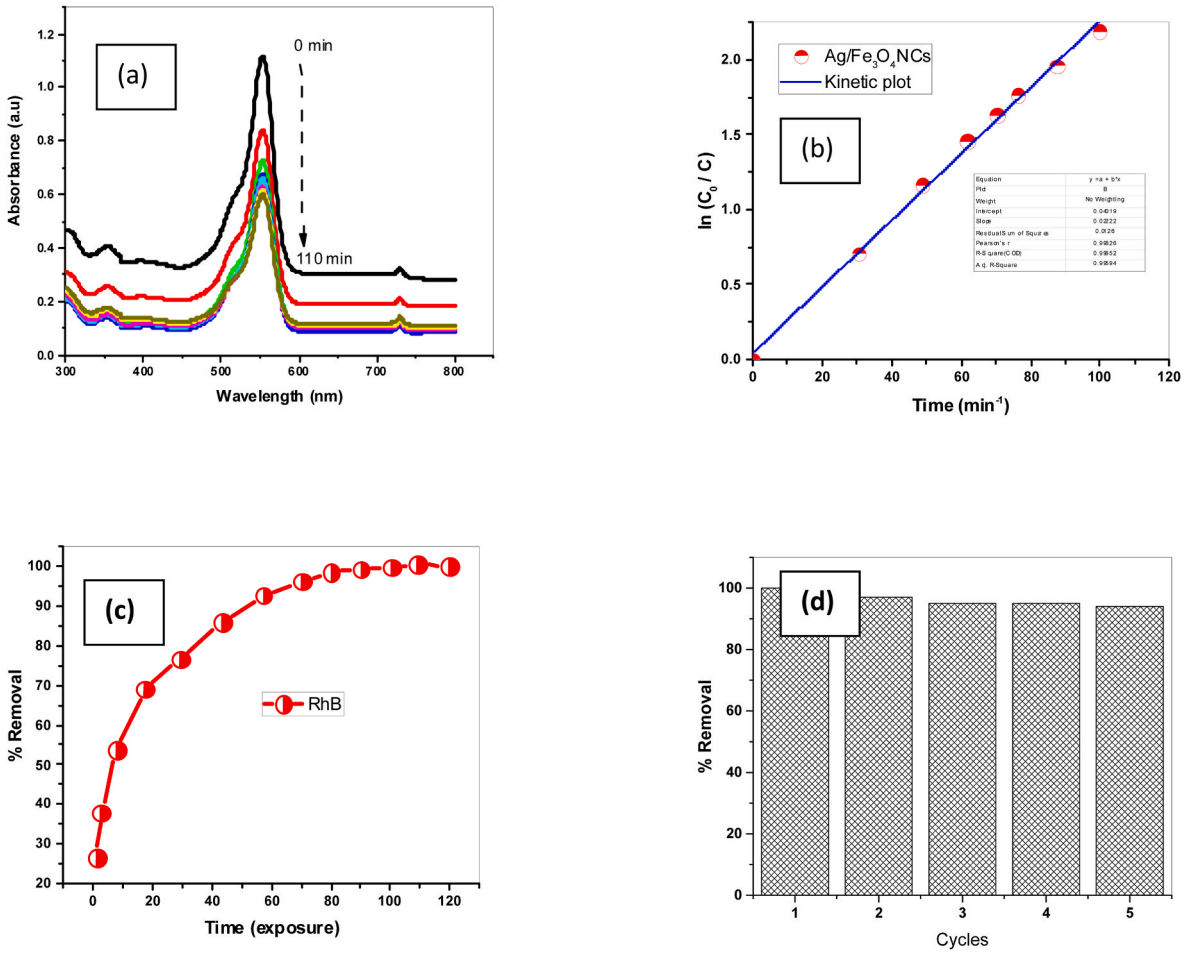

Fig. 6. **(a)** UV Absorption spectrum of Rhodamine B dye decompose (b) Kinetic plot (c) Percentage of dye removal (d) percentage of recyclability.

electron pair conjugation [33].

As a result, a larger number of electrons/holes take part in the photo degradation process. The enhanced photocatalytic activity of Ag/Fe_3O_4NCs under visible light irradiation was attributed to the suppression of charge recombination and enhanced charge separation in Ag. The increased photocatalytic activity resulted in the degradation of Rhodamine B within 110 min [40–44].

3.8.3. *Reusability of catalyst*

The immobilized catalyst could be easily recovered by magnetic separation and recycled for five times without significant loss of its catalytic activity [45,46].

3.9. *Bactericidal behavior*

An assay for the bacterial efficacy of streptomycin and Ag/Fe_3O_4NCs was examined at different concentrations (50, 75, 100 μL/mL) with two distinct gram positive bacteria, Escherichia coli and Bacillus subtilis, and two different gram negative bacteria, Pseudomonas aeruginosa and Staphylococcus aureus shown in Fig. 7 (a-d). When examining the four microbes probed, the prevalence of antibacterial action was quite obvious in the case of P. aeruginosa (24 mm) whereas E. coli (22 mm) displayed just moderate exercise, Staphylococcus aureus (19 mm) at 100 μL/mL of Ag/Fe_3O_4 as seen in Table 2. This could be sustained by the electrostatic forces of positively charged Ag/Fe_3O_4 NCs to the negatively charged exterior membrane of microorganism [47,48]. The findings revealed that JCR@Ag/Fe_3O_4 NCs produced a greater inhibitory effect than JCR due to their wider permeability, compact size, higher binding strength, but almost globular morphology of the nanoparticles, permitting synthesized Ag/Fe_3O_4 NCs to work effectively as an excellent antibiotic entity which can be beneficial in clinical field.

4. Conclusion

In this study, we designed and synthesized Ag/Fe_3O_4 NCs by using green bio-chelating agent using Fe_3O_4 and Ag NPs in a two-step protocol. The emergence of Ag/Fe_3O_4 MSC was acknowledged by XRD and electron microscopy outcomes. The Ag/Fe_3O_4NCs demonstrated excellent photocatalytic activity in the reduction of RhB dye, while retaining substantial catalytic activity upon reusing the catalyst. The detachment of Ag/Fe_3O_4NCs using an external magnetic field was a crucial and simple tool to investigate recovery and recycling without wasting catalyst. The diminishing reaction went before pseudo first solicitation energy, and the k_{app} was seen as of high changing, showing that Ag/Fe_3O_4 NCs has extraordinary development in heterogeneous conditions. The Ag/Fe_3O_4 NCs have incredible commitment of solid antibacterial movement against Gram-negative and Gram-positive pathogenic microorganisms, and their magnetostrictive property permitted them to be reused. Subsequently, evaluating the most important separation technique, financial, and environmental problems, and the use of such catalytic reactions may be useful for various biochemical reactions.

Funding

The authors declare that no funds, grants, or other support were received during the preparation of this manuscript.

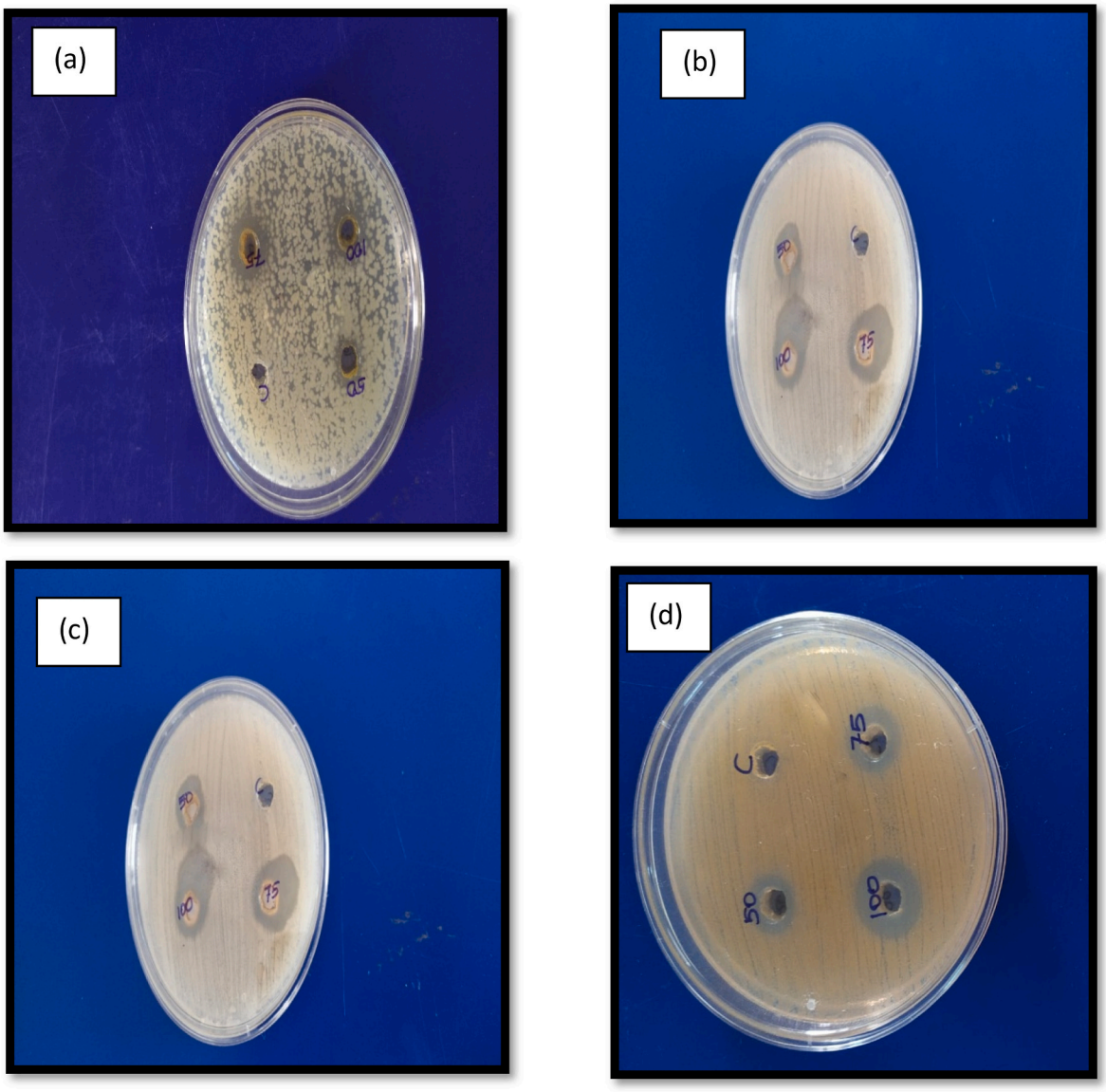

Fig. 7. Anti-bacterial action of synthesized Ag/Fe_3O_4 NCs **(a)** ***Bacillus subtilis*** (b) Staphylococcus aureus (c) Escherichia coli (d) Pseudomonas aeruginosa.

Table 1
Comparison of various nanomaterials used on Rhodamine B (Rh–B) DYE.

S. No	Material	time of exposure & % yield	references
1	Iron doped CeO_2 NCs	180 min, 92.6%	[34]
2	Fe_3O_4/TiO_2	120min, 100%	[35]
3	N–TiO2/$ZnFe_2O_4$	240min, 100%	[36]
4	zinc doped cobalt ferrite	210min, 99.9%	[37]
5	ZnO-Graphene oxide –TiO_2 NCs	170min, 95%	[38]
6	ceria based TiO2 nanomaterials	230min, 98%	[39]
7	Ag–Fe_3O_4 NCs	110min, 99.9%	present study

Data availability

Data sharing not applicable to this article as no datasets were generated or analyzed during the current study.

Table 2
Antibacterial activities of synthesized Ag/Fe_3O_4 NCs using Gram + ve and Gram –Ve strains.

S.No	Bacterial Strains	Inhibition Zone (mm)		
		50 μL/mL	75 μL/mL	100 μL/mL
1	Bacillus subtilis	7	9	11
2	Staphylococcus aureus	15	17	19
3	Escherichia coli	18	20	22
4	Pseudomonas aeruginosa	19	22	24

Declaration of competing interest

The authors declare that they have no known competing financial interests or personal relationships that could have appeared to influence the work reported in this paper.

References

[1] V.S. Shrivastava, Arch. Appl. Sci. Res. 3 (2012) 1244–1254.

[2] M Khatami, I Sharifi, MAL Nobre, N Zafarnia, MR Aflatoonian Green Chem. Lett. Rev. 11 (2), 125-134.
[3] M Khatami, S Pourseyedi, M Khatami, H Hamidi, M Zaeifi, L Soltani Biores. Bioprocess. 2 (1), 1-7.
[4] Mahmoud Nasrollahzadeh, S. Mohammad Sajadi, J. Colloid Interface Sci. 1 (469) (2016) 191–195.
[5] Akhil Tayala, Okkyun Seob, Jaemyung Kimb, Kohei Kusadac, Hirokazu Kobayashic, Hiroshi Kitagawac, Osami Sakata, J. Alloys Compd. 869 (2021), 159268.
[6] Yan Wang, Zhaoli Yan, Xiaodong Wang, Hindawi Pub. Corporat. Int. J. Photoenergy 4 (2014) 1–7.
[7] Patrick Wilhelm, Dietmar Stephan, J. Photochem. Photobiol. 185 (2007) 19–25.
[8] G. Hongwei, X. Keming, X. Chenjie, X. Bing, Chem. Commun. 9 (2006) 941–949.
[9] M.L. Chen, Y.J. He, X.W. Chen, J.H. Wang, Langmuir 28 (2012) 16469–16476.
[10] C. Alexiou, etal. Eur.Biophys.J 35 (2006) 446–450.
[11] L. Pana, L. Li, M. Xua, Z. Zhang, Mat. Sci. Eng. 176 (2011) 1123–1127 (B)).
[12] H. Byunghee, C. Namhyun, K.H. Kim, D.W. Lim, J. Choo, J. Phys. Chem. C115 (2011) 6290–6296.
[13] A. Chatzipavlidis, P. Bilalis, L.A. Tziveleka, N. Boukos, C.A. Charitidis, G. Kordas, Langmuir 29 (2013) 9562–9572.
[14] H. Xia, B. Cui, J. Zhou, L. Zhang, J. Zhang, X. Guo, H. Guo, Appl. Surf. Sci. 257 (2011) 9397–9402.
[15] S. Zhou, Q. Chen, Dalton Trans. 40 (2011) 8622–8629.
[16] Y.H. Deng, D.W. Qi, C.H. Deng, X.M. Zhang, D.Y. Zhao, J. Am. Chem. Soc. 130 (2008) 28–29.
[17] D.H. Zhang, G.D. Li, J.X. Li, J.S. Chen, Chem. Commun. (2008) 3414–3416.
[18] A. Amarjargal, L.D. Tijing, I.T. Im, C.S. Kim, Chem. Eng. J. 226 (2013) 243–254.
[19] B. Chudasama, A.K. Vala, N. Andhariya, R.V. Upadhyay, R.V. Mehta, J.Magn.Mater 323 (2011) 1233–1237.
[20] G. Lopes, etal. J.Phys.Chem C114 (2010) 10148–10152.
[21] Sada Venkateswarlu, B. NateshKumar, B. Prathima, K. Anitha, N.V.V. Jyothi, j. physb (2014), 09.007.
[22] Chaitali V. Khedkara, Nageshwar D. Khupse, Balu R. Thombarea, Pravin R. Dusanea, Gaurav Lole, Rupesh S. Devan, Aparna S. Deshpande, I. Shankar, Patila, chem. Phys. Lett. (2020), 137-131.
[23] G. Bharath Shoaib Anwer, R.V. Mangalaraja, Emad Alhseinat, Fawzi Banat, N. Ponpandian, Sci. Rep. 8 (2018) 5718.
[24] A. Tyurin, G. De Filpo, D. Cupelli, F.P. Nicoletta, A. Mashin, G. Chidichimo, Particle size tuning in silver-polyacrylonitrile nanocomposites, Express Polym. Lett. 4 (2010) 71–78.
[25] S. Nath, S. Kumar Ghosh, S. Praharaj, S. Panigrahi, S. Basu, T. Pal, Silver organosol: synthesis, characterisation and localised surface plasmon resonance study, New J. Chem. 29 (2005) 1527.
[26] F. Guo, H. Li, Z. Zhang, S. Meng, D. Li, Mater. Sci. Eng., B 163 (2009) 134–137.
[27] B. Gnanaprakasam, Akanksha M. Pandey, G. Sandip, Agalave, Chathakudath P. Vinod, Chem. Asian J. (2019), 00810.
[28] M. Fangzhi, G. Jianguo, M. Huiru, X. Leilei, S. Weidong, ACS Appl. Mater. Interfaces 4 (2012) 3987–3993.
[29] Y. Zhang, H. Ding, Y. Liu, S. Pan, Y. Luo, G. Li, J. Mater. Chem. 22 (2012) 10779–10786.
[30] J.P. Novak, D.L. Feldheim, J. Am. Chem. Soc. 122 (2000) 3979–3980.
[31] G. Bharath Shoaib Anwer, R.V. Mangalaraja, Emad alhseinat, Fawzi Banat & Ponpandian N, Sci. Rep. 8 (2018) 5718.
[32] M.R. Bindhu, P.V. Rekha, T. Umamaheswari, M. Umadevi, Mater. Lett. 131 (2014) 10–13.
[33] R. Gannimani, A. Perumal, S.B. Krishna, A. Mishra, K. Sershen, P. Muthusamy, N. Govender, Dig. J. Nanomater. Bios. 9 (2014) 1669–1679.
[34] Lianli Zou, Xiangqian Shen,Qiuju Wang,Zhou Wang, Xinchun Yang and Maoxiang Jing, J. Mater. Res. , Volume 30 , Issue 18 , 28 September 2015 , pp. 2763 – 2771.
[35] S. Xuan, W. Jiang, X. Gong, Y. Hu, Z. Chen, J. Phys. Chem. C 113 (2009) 553–558.
[36] Y. Yao, J. Qin, H. Chen, F. Wei, X. Liu, J. Wang, S. Wang, J. Hazard Mater. 291 (2015) 28–37.
[37] M. Sundararajan, V. Sailaja, L. John Kennedy, J. Judith Vijaya, Ceramics International Volume 43 (2017) 540–548. Issue 1, Part A, January.
[38] P. Nuengmatcha, S. Chanthai, R. Mahachai, W. Oh, J. Environ. Chem. Eng. 4 (2016) 2170–2177.
[39] K. Kasinathan, J. Kennedy, M. Elayaperumal, M. Henini, M. Malik, Sci. Rep. 38064 (2016) 1–12.
[40] Lekha Paramanik, K. Hemalata Reddy, Sabiha Sultana, Kulamani Parida, Architecture of Biperovskite-based LaCrO3/PbTiO3 p–n heterojunction with a strong interface for enhanced charge anti-recombination process and visible light-induced photocatalytic reactions inorg, Chem 57 (24) (2018) 15133–15148.
[41] Lekha Paramanik, a K. Hemalata Reddya, K.M. Parida, An energy band compactable B-rGO/PbTiO3 p–n junction: a highly dynamic and durable photocatalyst for enhanced photocatalytic H2 evolution, Nanoscale 11 (2019) 22328–22342.
[42] Lekha Paramanik, K. Hemalata Reddy, K.M. Parida, Stupendous photocatalytic activity of p-BiOI/n-PbTiO3 heterojunction: the significant role of oxygen vacancies and interface coupling, J. Phys. Chem. C 123 (35) (2019) 21593–21606.
[43] Samira Arefi-Oskoui, Alireza Khataee, Samira Jabbarvand Behrouz, Vahid Vatanpour, Samira Haddadi Gharamaleki, Yasin Orooji, Mahdie Safarpour, Development of MoS2/O-MWCNTs/PES blended membrane for efficient removal of dyes, in: antibiotic, and protein, Separation and Purification Technology 280, 2022, 119822.
[44] Yasin Orooji, Reza Akbari, Zahra Nezafat, Mahmoud Nasrollahzadeh, Taghi A. Kamali, Recent signs of progress in polymer-supported silver complexes/ nanoparticles for remediation of environmental pollutants, J. Mol. Liq. 329 (2021), 115583.
[45] Yasin Orooji, Reza Mohassel, Omid Amiri, Sobhani Azam, Masoud Salavati-Niasari, Gd2ZnMnO6/ZnO nanocomposites: green sol-gel auto-combustion synthesis, characterization and photocatalytic degradation of different dye pollutants in water, J. Alloys Compd. 835 (2020), 155240.
[46] Zahra Ansarian, Alireza Khataee, Samira Arefi-Oskoui, Yasin Orooji, Hongjun Lin, Ultrasound-assisted catalytic activation of peroxydisulfate on Ti3GeC2 MAX phase for efficient removal of hazardous pollutants, Mater. Today Chem. 24 (2022), 100818.
[47] Bahareh Feizi Mohazzab, Babak Jaleh*, Mahmoud Nasrollahzadeh*, Sadegh Khazalpour, Mohaddeseh Sajjadi, Rajender S. Varma, Upgraded valorization of Biowaste: laser-assisted synthesis of Pd/calcium lignosulfonate nanocomposite for hydrogen storage and environmental remediation, Cite this:ACS Omega 5 (11) (2020) 5888–5899.
[48] Mahmoud Nasrollahzadeh, Talat Baran, Nuray Yılmaz Baran, Mohaddeseh Sajjadi, Mohammad Reza Tahsili, Mohammadreza Shokouhimehr, Pd nanocatalyst stabilized on amine-modified zeolite: antibacterial and catalytic activities for environmental pollution remediation in aqueous medium, Separ. Purif. Technol. 239 (2020), 116542.